PCCP

Accepted Manuscript

ROYAL SOCIETY OF CHEMISTRY

www.rsc.org/pccp

Journal Name

RSCPublishing

ARTICLE

Two-dimensional molybdenum carbides: potential thermoelectric materials in MXenes

Cite this: DOI: 10.1039/xoxxoooooox

Mohamamd Khazaei,[a] Masao Arai,[a] Taizo Sasaki,[b] Mehdi Estili,[c] and Yoshio Sakka[d]

Received ooth January 2012,
Accepted ooth January 2012

DOI: 10.1039/xoxxoooooox

www.rsc.org/

Newly synthesized family of two-dimensional transition metal carbides and nitrides, so-called MXenes, attain metallic or semiconducting properties upon proper surface functionalization. Owing to their intrinsic ceramic nature, MXenes may be suitable for energy conversion applications at high temperature. Using the Boltzmann theory and first-principles electronic structure calculations, we explore the thermoelectric properties of monolayer and multilayer M_2C (M = Sc, Ti, V, Zr, Nb, Mo, Hf, Ta) and M_2N (M= Ti, Zr, Hf) MXenes functionalized by F, OH, and O groups. From our calculations, it turns out that monolayer and multilayer nanosheets of Mo_2C acquire superior power factors to other MXenes upon any type of functionalization. We thereby propose the functionalized Mo_2C nanosheets as potential thermoelectric materials in the MXene family. The exceptional thermoelectric properties of the functionalized Mo_2C nanosheets is attributed to the peculiar t_{2g} band shapes, which are combined of flat and dispersive portions. This type of the band shapes allows Mo_2C to gain a large Seebeck coefficient and simultaneously a good electrical conductivity at low carrier concentrations

1. Introduction

Owing to the technological applications of thermoelectric materials in clean power generation from waste-heat sources such as power plants and car engines, the search for high-performance thermoelectric materials has become one of the current subjects of interest in materials science.[1] The performance of a thermoelectric material is quantified through the dimensionless figure of merit ZT given by $S^2\sigma T/\kappa$, where S, σ, T, and κ are the Seebeck coefficient, electrical conductivity, temperature, and thermal conductivity ($\kappa = \kappa_l+k_e$) with both lattice (κ_l) and electronic (k_e) contributions, respectively. The best thermoelectric materials available today, operating near room temperature, are doped semiconductor alloys of antimony and bismuth telluride, which have ZT of about 1.[1,2] A thermoelectric material with ZT of 1 operates at only 10% of Carnot efficiency,[3] which might still be worth for some industrial applications. Nevertheless, for practical purposes, a thermoelectric material with ZT of at least 4, which is comparable to home refrigeration with 30% of Carnot efficiency, is desired.[3] Though scientists have already developed many approaches to enhance the performance of thermoelectric materials,[1] the increase of ZT by a factor of 4 has remained a formidable challenge.

Efficiency, stability, production cost, and environmental effect are the essential factors that determine the range of applicability of a thermoelectric material. Heavy or rare elements such as tellurium are expensive ($552/500gr, Kojundo Chemical Laboratory Co. Ltd., 2013) and toxic. Therefore, it might unlikely be used in large-scale applications.[4] Considering their availability and superior thermal stability in air,[5,6] a family of the layered solids called MAX phases with ceramic nature might attract attentions for examining their possible thermoelectric applications at high temperatures. In detail, the MAX phases form a large family of layered metallic solids with chemical formula of $M_{n+1}AX_n$, where n = 1, 2, or 3, "M" is an early transition metal (Sc, Ti, V, Cr, Zr, Nb, Mo, Hf, Ta), "A" is an element from groups 13-16 in the periodic table (Al, Si, P, S, Ga, Ge, As, In, Sn, Tl, Pb), and "X" is carbon and/or nitrogen.[5] However, previous experiments and theoretical calculations indicated that the MAX phases are poor thermoelectric materials.[7-10] This is because metallic systems typically gain small Seebeck coefficients.

Recently, experimentalists succeeded to exfoliate the MAX phases into two-dimensional sheets through selective etching of "A" layers by using appropriate hydrofluoric acids.[11-17] The obtained two-dimensional carbide or nitride system is called MXene, which is typically functionalized by hydroxyl, oxygen, and fluorine groups. In this regard, first principles calculations have revealed that the electronic structures of the MXenes differ substantially from their original MAX phases;[18-25] some of the M_2C (M = Sc, Ti, V, Cr, Zr, Nb, Hf, Ta) MXenes upon functionalization with F, OH, and O turn from metallic into semiconducting nature with band gaps between 0.24 to 1.8 eV.[23-25] For the semiconducting MXenes, Sc_2CF_2, $Sc_2C(OH)_2$, Sc_2CO_2, Ti_2CO_2, Zr_2CO_2, and Hf_2CO_2, it has been predicted to attain large Seebeck coefficients at low temperatures.[24] Therefore, the MXenes might achieve better thermoelectric efficiencies than their original MAX phases. Here, we extensively study the thermoelectric properties of the MXene family theoretically by providing quantitative predictions and presenting the physical pictures behind them.

Thermoelectric properties — the Seebeck coefficient, the electrical conductivity, and the power factor ($S^2\sigma$) — of monolayers and multilayers of the functionalized M_2C (M = Sc, Ti, V, Zr, Nb, Mo, Hf, Ta) and M_2N (M = Ti, Zr, Hf) nanosheets with F, OH, and O groups are investigated by using first-principles calculations and the Boltzmann theory.[26] The calculation results suggest that monolayer and multilayer of

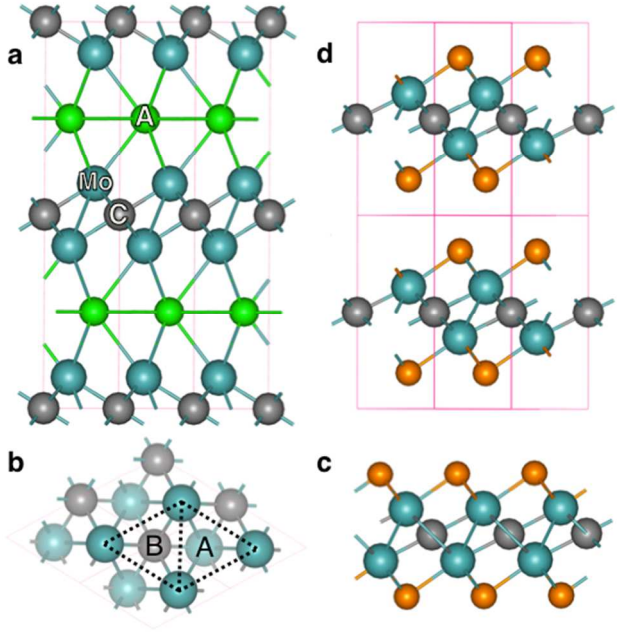

Fig. 1 (a) Structure of a typical Mo_2AC MAX phase. (b) Top view of a pristine 2D-Mo_2C system. A and B indicate two different hollow sites. (c) and (d) are side views of monolayer and multilayer Mo_2CF_2 (model 2).

functionalized Mo_2C attain larger power factor than all other MXenes. In particular, Mo_2CF_2 with a narrow semiconducting-gap ~0.25 eV is probably the most promising thermoelectric material among all the studied MXenes. Owing to remarkable thermoelectric properties of the Mo_2C family, we devote the results-and-discussion section of this paper to fully understand the relationship between the electronic and excellent thermoelectric properties of functionalized Mo_2C nanosheets: after discussion on the effects of functional groups on the electronic properties of the Mo_2C nanosheets, we examine and compare the thermoelectric properties of all the MXenes together.

2. Method of calculations

First-principles calculations were performed within the framework of the density functional theory (DFT) with the Perdew-Burke-Ernzerhof (PBE) version of the generalized-gradient approximation (GGA) as the exchange-correlation functional.[27] The projector augmented wave method (PAW) was used for the basis set as was implemented in the VASP code.[28] In the calculations, we used a plane-wave cutoff energy of 520 eV. The positions of atoms and the cell parameters were fully optimized by using the conjugate gradient method and applying the Methfessel-Paxton smearing scheme with the smearing width of 0.1 eV.[29] In the optimized structures, the magnitude of the force acting on each atom became less than 0.005 eV/Å. The total energies of the optimized structures were well-converged, 10^{-6} eV/cell. In the structural optimizations of monolayers and multilayers, the Brillouin zone was sampled using a set of 12×12×1 and 12×12×6 Monkhorst-Pack *k* points,[30] respectively. The electronic structures and thermoelectric properties were obtained using 80×80×1 and 48×48×12 *k* points and using the tetrahedron method. In order to avoid any interaction between a monolayer and its images along the *c* axis, a vacuum space of 30 Å was used.

Here, thermoelectric transport properties — the Seebeck coefficient (S), the electron conductivity (σ), and the power factor ($S^2\sigma$) — were computed within the Boltzmann theory[26] and the constant relaxation time (τ) approximation. Within this approximation, the Seebeck coefficient becomes τ-independent without any other adjustable parameter, but the electrical conductivities and thus the power factors are obtained with respect to τ. Based on this approximation, the electrical conductivity and Seebeck coefficient tensors of a material can be written as

$$\sigma_{\alpha\beta}(T,\mu) = \frac{1}{\Omega}\int \bar{\sigma}_{\alpha\beta}\left[-\frac{\partial f_\mu(T,\varepsilon,\mu)}{\partial\varepsilon}\right]d\varepsilon$$

$$S_{\alpha\beta}(T,\mu) = \frac{1}{eT\Omega\sigma_{\alpha\beta}(T,\mu)}\int \bar{\sigma}_{\alpha\beta}(\varepsilon-\mu)\left[-\frac{\partial f_\mu(T,\varepsilon,\mu)}{\partial\varepsilon}\right]d\varepsilon$$

$$\bar{\sigma}_{\alpha\beta} = \frac{e^2}{N}\sum_{i,\mathbf{k}}\tau v_\alpha(i,\mathbf{k})v_\beta(i,\mathbf{k})\delta(\varepsilon-\varepsilon_{i,\mathbf{k}})$$

where α and β are tensor indices, Ω, μ and *f* are the volume of the unit cell, chemical potential, and the Fermi-Dirac distribution function, respectively, and *e* is the electron charge. *N* indicates the number of **k** points sampled. In the formulations $v_\alpha(i,\mathbf{k})$ ($\alpha = x, y, z$) is the αth component of the group velocity of carriers ($=1/\hbar\nabla_{\mathbf{k}}\varepsilon_{i,\mathbf{k}}$). The above formulations have already been implemented in BoltzTrap code.[31-33] The details of implementations can be seen in references 31-33. All the calculations were performed with the above code. We checked the reliability of our calculations, by examining S, σ/τ, and $S^2\sigma/\tau$ for TiCoSb, ZrNiSn, and LaPdBi.[33] The results are in excellent agreement with the previous calculations as demonstrated in supporting information file.[33] In order to find the doping effect on the thermoelectric properties, we assumed the rigid band approximation, where the chemical potential (μ) determines the number of carriers and its shift to higher or lower energies mimics the effect of *n* or *p* dopants.[31-33]

3. Results and discussion

3.1 Structural and electronic properties of 2D-Mo_2C upon chemical functionalization

A 2D Mo_2C sheet may be formed from the exfoliation of a 3D Mo_2AC in the MAX phase solids (depicted in Fig. 1a) by eliminating the "A" elements using a proper acid solution. For instance, it was predicted that Mo_2InC, which has the lowest exfoliation energy and the highest elastic constant anisotropy between C_{11} and C_{33}, might be a suitable candidate for the exfoliation process to obtain 2D Mo_2C nanosheets.[34] The unit cell of pristine 2D Mo_2C possesses hexagonal lattice and includes two Mo atoms and one C atom forming a three atomic layer structure in which the carbon layer is sandwiched between two Mo layers. During the exfoliation process in the experiments, the surfaces of MXenes are functionalized by F, OH, and/or O groups because of the utilized hydrofluoric acid solution.[11,12] In the previous theoretical study, it was predicted that the MXenes with full surface functionalizations are thermodynamically more favorable than less functionalizations.[24] Hence, since in Mo_2C sheets both Mo atoms locate on the surfaces, two F, OH, or O chemical groups are required for the full surfaces functionalization. For better understanding of the electronic and chemical changes of the Mo_2C upon functionalization with F, O, and

OH, we have also investigated the effects of other chemical groups, Cl, Br, and S.

There are several possibilities for the functionalization of an MXene.[24] On each surface of the MXene, two types of hollow sites exist (Fig. 1b): the hollow sites without and with carbon atom available under it, which are denoted as A and B, respectively. Therefore, according to the relative positions of the attached chemical groups to the Mo atoms, four different configurations are possible for the chemical terminations of the Mo_2C system. Model 1: two functional groups locate on the top of two Mo atoms. Model 2: the two functional groups are at the hollow sites A (Fig. 1c). Model 3: one of the functional groups locates at the hollow site A and the other functional group at the hollow site B. Model 4: two functional groups locate at the hollow sites B. To determine the most stable configuration for each type of the functionalization, the atomic positions and lattice parameters of the above four models are fully optimized. The most stable configurations of the studied MXenes can be found in the supporting information file.

Table 1. Total energies (eV/cell) of Mo_2C with models 1-4 upon different types of functionalization. Total energy of the most stable model is indicated in bold. Formation energies (eV/cell) are calculated by using the total energies of the most stable model.

Functionalized Mo2C	Model 1	Model 2	Model 3	Model 4	Formation energy
Mo_2CF_2	-39.726	**-40.042**	-39.544	-39.718	-7.808
Mo_2CCl_2	-35.949	**-36.793**	-36.263	-36.328	-4.703
Mo_2CBr_2	-34.453	**-35.422**	-35.422	-.34.707	-3.904
$Mo_2C(OH)_2$	-51.964	**-52.009**	-51.602	-51.817	-6.861
Mo_2CO_2	-43.576	-45.177	-45.591	**-46.281**	-7.905
Mo_2CS_2	-38.367	-41.059	-41.276	**-41.783**	-6.111

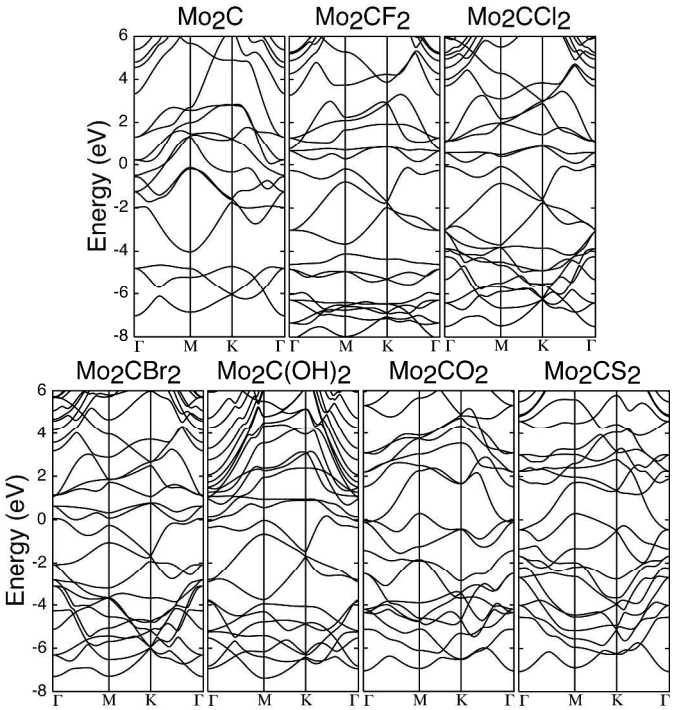

Fig. 2 Band structures of pristine and functionalized Mo_2C with F, F, Cl, Br, OH, O, and S. Γ(0,0), M(1/2,0), and K(1/3,1/3) are symmetry points of the Brillouin zones for a hexagonal lattice. The energy zero is set to be the top of the highest occupied level.

From total energy results in Table 1, it is observed that model 2 is the most stable for Mo_2CF_2, Mo_2CCl_2, Mo_2CBr_2, and $Mo_2C(OH)_2$ while the model 4 is the most sable for Mo_2CO_2 and Mo_2CS_2. Functionalized Mo_2C with F, Cl, Br, and OH prefer similar model and that with O and S do. This corresponds to the fact that F, Cl, Br, and OH analogously demand one electron to complete their electronic shells, but O and S demand two. With a particular functionalization, the preference of a model to other models is controlled by several entangled factors such as the oxidation state of the transition metal, the number of demanded electrons by the functional groups, and the strength of hybridizations between the functional group and transition metal.[24]

In order to consider the stability of the functionalized Mo_2C sheets, we have calculated their formation energies defined by $\Delta H_f = E_{tot}(Mo_2CY_2) - E_{tot}(Mo_2C) - E_{tot}(Y_2)$, where Y= F, Cl, Br, OH, O or S groups. $E_{tot}(Mo_2C)$ and $E_{tot}(Mo_2CY_2)$ stand for the total energies of pristine and functionalized Mo_2C, respectively. Depending on the functionalization type, $E_{tot}(Y_2)$ is the total energy of F_2, Cl_2, Br_2, O_2+H_2, O_2, or S_2. The calculated formation energies are presented in Table 1. It is observed that all cases have large negative formation energies. This indicates the creation of strong bonds between 2D Mo_2C and the attached groups, which result in surface functionalization of Mo_2C. Since the formation energies of Mo_2CF_2, $Mo_2C(OH)_2$, Mo_2CO_2, and Mo_2CS_2 are larger than those of Mo_2CCl_2 and Mo_2CBr_2, probably their experimental productions may be more feasible.

Structurally, the functionalized Mo_2C systems can be considered as kinds of octahedral (represented by model 2) or trigonal-like (represented by model 4) compounds in which each Mo atom is surrounded by three carbon atoms and by three attached chemical groups. But they have lower symmetries because the bond distances of Mo with surrounding carbon atoms differ from the bond distances of Mo with surrounding chemical groups.

Figs. 2 and 3 show the band structures and the local density of states (LDOSs) of the pristine and functionalized Mo_2C with F, Cl, Br, OH, O, and S. It is seen that pristine Mo_2C, Mo_2CBr_2, $Mo_2C(OH)_2$, Mo_2CO_2, and Mo_2CS_2 are metallic, but Mo_2CF_2 and Mo_2CCl_2 are semiconducting with narrow indirect band gaps of 0.27 and 0.15 eV, respectively. Precisely Mo_2CBr_2 and $Mo_2C(OH)_2$ are semi-metallic. As a notable case, in order to investigate the contribution ofeach atomic orbitals in LDOS, the projected densities of states (PDOS) of Mo_2CF_2, which are actually decomposed LDOS onto angular momentum channels, are shown in Figs. 3c-e. From the band structure and LDOS of pristine Mo_2C, it is seen that due to hybridization between C-s and Mo-d orbitals, the C-s band is formed around -12.5 eV (not shown in the energy range of Figs. 2 and 3). The C-p bands, which result from hybridization between C-p and Mo-d orbitals, are created at energies between -7.0 and -5.0 eV. The states near Fermi energy result mainly from the hybridization between Mo-d orbitals. The states above 4.0 eV include the anti-bonding states between C-p and Mo-d orbitals.

Upon F, Cl, Br, OH, O, and S functionalization, s and p orbitals of the attached chemical groups are hybridized with the Mo-d and C-p orbitals (Fig. 3). Consequently several new states are created below the Fermi energy of pristine Mo_2C. Two attached chemical groups form degenerate s-bands below the C-s band at energies around -24.0 eV (not shown in the figures) and form six p-bands below the C-p bands. For example, in the band structure of Mo_2CF_2 whose six F-p bands can be seen at energies between -8.0 and -6.0 eV. From PDOSs in Figs. 3b-e, it is seen that the hybridizations between C-p and F-p orbitals are also noticeable. More precisely, three C-p and six F-p bands together form nine dispersed-entangled bands in which both C-p and F-p orbitals contribute significantly. This is clearer in the band structures and

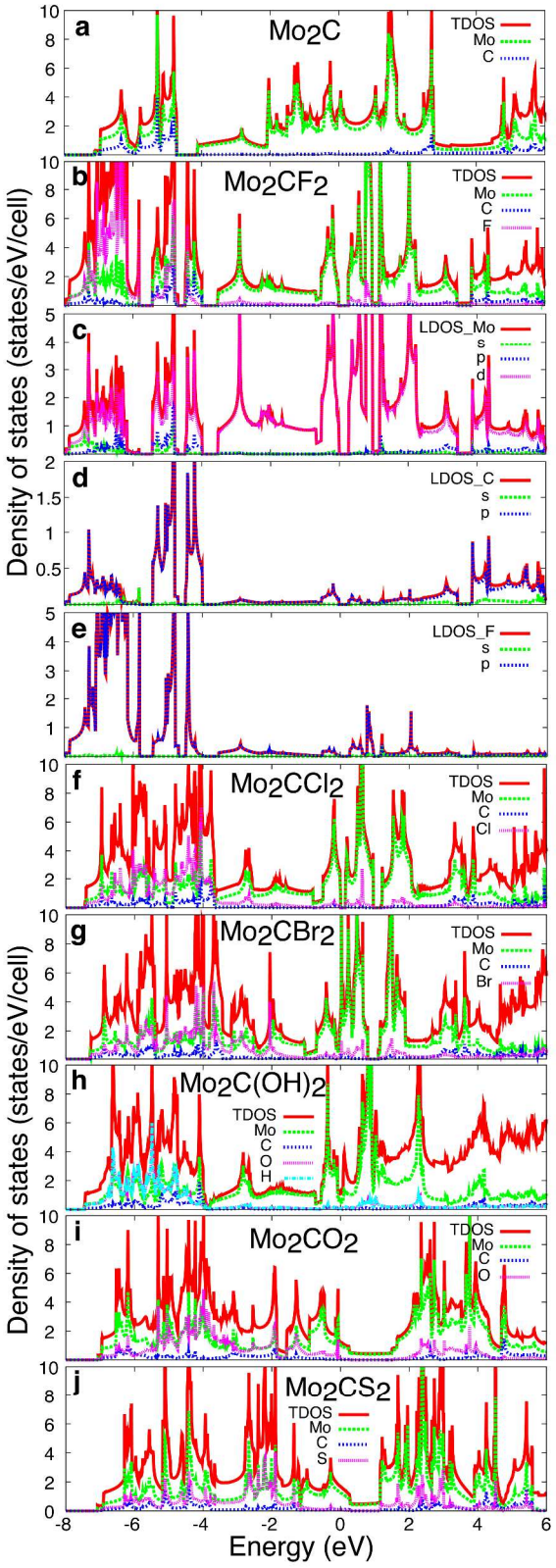

Fig. 3 (a), (b), and (f)-(j) total and local density of states of pristine Mo_2C, and functionalized Mo_2C with F, Cl, Br, OH, O, and S. (c)-(e) projected densities of states of Mo_2CF_2 on different atoms and different atomic orbitals. The energy zero is set to be the top of the highest occupied level.

LDOS of Mo_2C systems functionalized with Cl, Br, O, and S. For the case of Mo_2CO_2/Mo_2CS_2, the hybridizations between C-p and O-p/S-p orbitals are even more pronounced because in model 4 the attached chemical groups locate at the hollow sites, where the carbon atoms exist under them. Consequently, the C-p_z and O-p_z/S-p_z can become hybridized strongly.

The energy bands around the Fermi energy of the functionalized Mo_2C systems originate mainly from the Mo d-orbitals. The splitting and dispersion of these energy bands are largely affected by the strength of covalency (resulting from hybridizations) and ionicity (resulting from different electronegativity) of the bonds between Mo and the attached chemical groups. It is seen that though functionalized Mo_2C with F, Cl, Br, and OH possess similar structures (model 2), their electronic properties are different; Mo_2CF_2 and Mo_2CCl_2 are semiconducting, while the others are metallic. Such ligand dependence electronic structures are often seen in transition metal-based compounds with octahedral or trigonal symmetries.[35] In such compounds, due to hybridizations and ligand fields, the five d levels of a transition metal atom split into two main groups: three t_{2g} levels and two e_g levels. Indeed, the traces of such splitting is seen in functionalized Mo_2C systems; the three occupied d bands of Mo_2CF_2 and Mo_2CCl_2 are mainly composed of t_{2g} orbitals (in the energy region between -4.0 and 0.0 eV), which are separated from other seven lowest unoccupied d bands by small energy gaps. However, these band gaps cannot be explained only by t_{2g} and e_g splitting. Actually, in the functionalized Mo_2C systems, due to the low symmetries of the structures, degeneracy of states are lifted. In such circumstances the functionalized Mo_2C systems become either metallic or semiconducting with fairly small band gaps.

3.2 Thermoelectric properties of functionalized MXenes

We have examined the thermoelectric properties of monolayers and multilayers of functionalized M_2C (M = Sc, Ti, V, Zr, Nb, Mo, Hf, Ta) and M_2N (M= Ti, Zr, Hf) with F, O, and OH on the basis of the Boltzmann theory and a set of first-principles calculations. Though the relaxation time is an undetermined constant parameter in the calculations, still the comparison of the thermoelectric properties of the MXenes can be justified. This is because all MXenes have similar hexagonal structures and all of them originally belong to the same family of materials, the MAX phases. Therefore, it can be expected that the electron scattering mechanisms in the MXenes are similar, and thus, their relaxation time can be assumed to be in the same order (please see more justifications at the end of supporting information file). This makes the comparison of the thermoelectric results meaningful. We present the calculation results of DOS and the thermoelectric properties at different temperatures in the range of 300-600 K and different carrier concentrations for all considered monolayers and multilayers in the supplementary file.

In the calculations, the multilayer systems are modelled by three-dimensional close stack of the functionalized monolayers (Fig. 1d). It turns out that there are no significant differences between the monolayers and their corresponding multilayer structures in the electronic and thermoelectric behaviours. This indicates that the interactions between the layers in multilayer MXenes are relatively weak. The only exceptional case is $Mo_2C(OH)_2$; due to the stacking of the layers, its multilayer system becomes semiconductor with a small gap around 0.1 eV. It should be noted that the direct comparison of electrical conductivities and thermo factors of monolayers with multilayers are not possible because these quantities

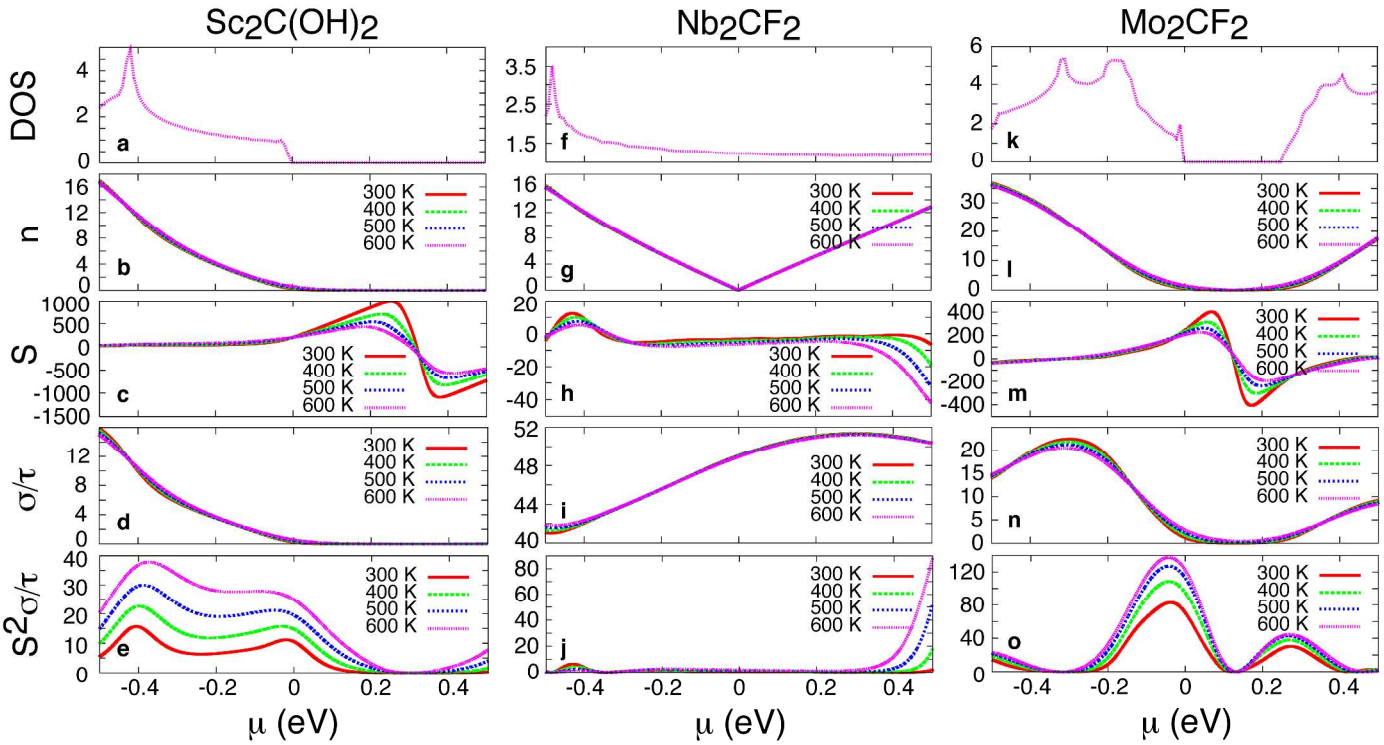

Fig. 4 Density of states (DOS [states/eV/cell]), carrier density (n [10^{20}cm^{-3}]), Seebeck coefficient (S [μVK^{-1}]; $S = (S_{xx}+S_{yy}+S_{zz})/3$), electrical conductivity (σ/τ [10^{17}Ω^{-1}cm^{-1}s^{-1}]; σ =($\sigma_{xx}+\sigma_{yy}+\sigma_{zz}$)/3), and power factor ($S^2$σ/τ [$10^{14}$μWcm^{-1}K^{-2}s^{-1}]) as a function of the chemical potential at various temperatures for multilayers of $Sc_2C(OH)_2$ (a-e), Nb_2CF_2 (f-j), and Mo_2CF_2 (k-o). μ =0 is set to be at the original highest occupied level. It is noted that both valence and conduction bands have been included in the transport calculations, but the results were shown only for the range of chemical potentials between -0.5 and 0.5 eV.

Table 2. Electronic and thermoelectric properties of various functionalized MXenes with F, OH, and O at 400 K. The maximum power factor (Max PF) is in the unit of $\tau\times10^{14}$ W cm^{-1} K^{-2} s^{-1}. The chemical potentials (CP) and their corresponding p and n doping levels are in the unit of eV and e/unit cell. CPs indicate the energy positions where Max PFs were extracted. Max PFs are searched in CPs between 0.3 below and above the Fermi energy. Some of the MXenes have just one Max PF. The absent Max PF and its related CP are indicted by slashes.

MXene	Sc_2CF_2	$Sc_2C(OH)_2$	Ti_2CF_2	$Ti_2C(OH)_2$	Ti_2CO_2	Ti_2NF_2	$Ti_2N(OH)_2$	Ti_2NO_2	V_2CF_2
Gap (eV)	1.0	0.71	0.0	0.0	0.17	0.0	0.0	0.0	0.0
Max PF (p)	17.564	15.737	8.517	24.106	6.182	2.197	9.505	18.223	0.216
Max PF (n)	/	/	1.786	/	30.526	0.482	2.596	12.229	1.252
CP/p-Doping	-0.027/0.0056	-0.031/0.0050	-0.069/0.0206	-0.020/0.0049	-0.3/0.0054	-0.091/0.0177	-0.3/0.0826	-0.3/0.123	-0.175/0.0525
CP/n-Doping	/	/	0.130/0.0384	/	0.226/0.0046	0.033/0.0086	0.050/0.0155	0.149/0.0867	0.199/0.0619

MXene	$V_2C(OH)_2$	V_2CO_2	Hf_2NF_2	$Hf_2N(OH)_2$	Hf_2NO_2	Ta_2CF_2	$Ta_2C(OH)_2$	Ta_2CO_2	Zr_2CF_2
Gap (eV)	0.0	0.0	0.0	0.0	0.0	0.0	0.0	0.0	0.0
Max PF (p)	1.45	11.083	9.17266	/	1.411	2.782	1.704	2.966	10.285
Max PF (n)	16.116	11.28	3.59	6.9	10.988	0.162	/	1.653	/
CP/p-Doping	-0.3/0.0914	-0.185/0.0432	-0.173/0.137	/	-0.3/0.06379	-0.191/0.034	-0.141/0.0787	-0.3/0.0407	-0.112/0.0206
CP/n-Doping	0.161/0.0530	0.3/0.0971	0.3/0.2027	0.023/0.0389	0.246/0.0662	0.3/0.0467	/	0.244/0.0340	/

MXene	$Zr_2C(OH)_2$	Zr_2CO_2	Zr_2NF_2	$Zr_2N(OH)_2$	Zr_2NO_2	Nb_2CF_2	$Nb_2C(OH)_2$	Nb_2CO_2	Mo_2CF_2
Gap (eV)	0.0	0.66	0.0	0.0	0.0	0.0	0.0	0.0	0.25
Max PF (p)	19.279	22.961	/	25.742	5.190	1.710	/	4.059	108.486
Max PF (n)	/	/	32.659	/	10.5	/	42.156	1.055	37.887
CP/p-Doping	-0.175/0.0275	-0.039/0.017	/	-0.202/0.0561	-0.3/0.0867	-0.23/0.0440	/	-0.3/0.048	-0.042/0.0131
CP/n-Doping	/	/	0.221/0.0347	/	0.3/0.0917	/	0.095/0.021	0.25/0.039	0.270/0.0089

MXene	Mo_2CCl_2	Mo_2CBr_2	$Mo_2C(OH)_2$	Mo_2CO_2	Mo_2CS_2	Hf_2CF_2	$Hf_2C(OH)_2$	Hf_2CO_2
Gap (eV)	0.05	0.0	0.1	0.0	0.0	0.0	0.0	0.8
Max PF (p)	70.938	32.140	99.913	/	37.72	16.664	13.105	16.2487
Max PF (n)	20.806	/	45.4	82.055	11.931	1.865	1.8625	/
CP/p-Doping	-0.103/0.0447	-0.216/0.05867	-0.061/0.01506	/	-0.044/0.0239	-0.144/0.0219	-0.3/0.0381	-0.0268/0.001
CP/n-Doping	0.115/0.01394	/	0.206/0.00814	0.217/0.0674	0.094/0.0426	0.158/0.0284	0.074/0.0103	/

are volume dependent; the thickness (consequently the volume) of a monolayer cannot be well determined. Since the exfoliated MXenes prefer the multilayer form in the experiments,[11,12] we preferably present the results for the multilayers here. Table 2 summarizes the results for the maximum power factors that can be obtained by optimizing the chemical potentials of the *p*- or *n*-type doped functionalized multilayer MXenes at 400 K — the temperature that many applications can be expected for thermoelectric materials in fuel cells and car engines. The data in Table 2 were obtained for the chemical potentials in the range of 0.3 eV below and above the original highest occupied level, where the carrier concentrations are typically less than 10^{21} cm^{-3} and maybe the rigid-band approximation is applicable.

Table 2 shows that functionalized Mo_2C with F, Cl, Br, OH, O, and S attain larger power factors than all other functionalized MXenes: in particular, Mo_2CF_2 and $Mo_2C(OH)_2$ with the highest power factors can be considered as the most promising thermoelectric materials in the family of the MXenes. In contrast, V_2CF_2, Nb_2CF_2, Nb_2CO_2, Ta_2CF_2, $Ta_2C(OH)_2$, and Ta_2CO_2 exhibit the lowest power factors among all considered MXenes, indicating poor thermoelectric properties. In order to obtain better understanding of the thermoelectric properties of the MXenes, we show DOS, carrier density, S, σ/τ, and $S^2\sigma/\tau$ of multilayer Mo_2CF_2, $Sc_2C(OH)_2$, and Nb_2CF_2, with the largest, average, and the lowest power factors, respectively, as a function of the chemical potential and different temperatures 300-600 K in Fig. 4.

Generally, ZT can be maximized when the power factor is maximized and the thermal conductivity is minimized conversely. The thermal conductivity can be minimized efficiently by enhancing the phonon scatterings by the edges, interfaces, grain boundaries, and embedded nanostructures.[36-38] But, maximizing $S^2\sigma$ is not straightforward because both S and σ are strongly coupled to the electronic structure of the system and usually behave inversely: materials that have high Seebeck coefficients have poor electrical conductivity, and vice versa. Therefore a balance between the Seebeck coefficient and the electrical conductivity at a particular *p*- or *n*-type carrier concentration is demanded so as to maximize the power factor, as was indicated before in Table 2.

From the $S^2\sigma/\tau$ results of the MXenes in Fig. 4, it is found that Mo_2CF_2 at temperatures above 300 K with a band gap of 0.25 eV deserves a large Seebeck coefficient, and relatively good electrical conductivity at low hole carrier concentrations, and consequently large $S^2\sigma/\tau$. $Sc_2C(OH)_2$ with a larger band gap (0.71 eV) obtains a larger Seebeck coefficient than Mo_2CF_2, but a smaller conductivity near its band edges. Overall, $Sc_2C(OH)_2$ obtains a smaller power factor than Mo_2CF_2. Nb_2CF_2 is a metallic system with better electrical conductivity than Mo_2CF_2 and $Sc_2C(OH)_2$. However, it obtains a small Seebeck coefficient. Thereby, Nb_2CF_2 exhibits poor thermoelectric properties. From our calculations, it is found that all semiconducting MXenes, Sc_2CF_2, $Sc_2C(OH)_2$, Ti_2CO_2, Zr_2CO_2, Mo_2CF_2, Mo_2CCl_2, $Mo_2C(OH)_2$, and Hf_2CO_2, obtain large Seebeck coefficients (>100 μV/K at 400 K) near the band edges.

The effect of a band gap on enhancement of the Seebeck coefficient can be understood through its formula.[31-33] The Seebeck coefficient is proportional to $\frac{\nu}{\sigma}$, where σ is the electrical conductivity and ν is the $(\varepsilon-\mu)$ weighted by average value of squared band velocities of electrons multiplied by DOS and derivative of the Fermi function ($f(\varepsilon)$) with respect to the energy ($df(\varepsilon)/d\varepsilon$). The $(\varepsilon-\mu)$ $df(\varepsilon)/d\varepsilon$ has opposite signs in the energy regions above and below the chemical potential.[31] Thus, it can be easily understood that S tends to be large once the DOS and band velocities at above and below the chemical potential have big contrast.[39,40] Accordingly, if the chemical potential locates in the energy region where the DOS and band velocities change smoothly, the Seebeck coefficient would be small due to the cancellation of the positive and negative contributions. This is the reason why Nb_2CF_2 with a smooth DOS near the original Fermi level obtains a negligible Seebeck coefficient (Figs. 4f and 4h). In semiconducting materials, as the chemical potential moves toward the band edges, the difference between the number of states above and below the chemical potential increases, which results in the increase in S. By this reason, the semiconducting MXenes such as $Sc_2C(OH)_2$ and Mo_2CF_2 obtain large Seebeck coefficients near the band edges (Figs. 4c and 4m).

From our calculations it is seen that $Sc_2C(OH)_2$ with a larger band gap (0.71 eV) than Mo_2CF_2 (0.25 eV) obtains a larger Seebeck coefficient near band edges (Figs. 4c and 4m). The same trend is seen in other semiconducting MXenes with different band gaps. To explain the above observation, it should be noted that $(\varepsilon-\mu)$ $df(\varepsilon)/d\varepsilon$ is a broad function;[31] the bands which are in the range of $\sim 5k_BT$ around the chemical potential can contribute to the Seebeck coefficient effectively.[41] Since in semiconductors the contributions from valence- and conduction-band states near the band edges to the Seebeck coefficient are opposite in sign, semiconductors with narrower band gaps obtain smaller Seebeck coefficients: the larger a band gap is, the larger Seebeck coefficient is probably to be achieved.

In Fig. 4, it is seen that the Seebeck coefficients values of semiconducting MXenes are sensitive to the temperature. Indeed, S decreases as the temperature increases from 300 to 600 K. As pointed out in the last paragraph, the decrease in S at high temperatures at low carrier concentration level is due to the minority-carrier contribution (with opposite sign contribution in Seebeck coefficient) in the range of $\sim 5k_BT$, as is often the case for narrow band-gap semiconductors.[42]

Fig. 5 Typical band structures of semiconducting MXenes. Γ(0,0), M(1/2,0), and K(1/3,1/3) are symmetry points of the Brillouin zone. The valence band maximum is at zero.

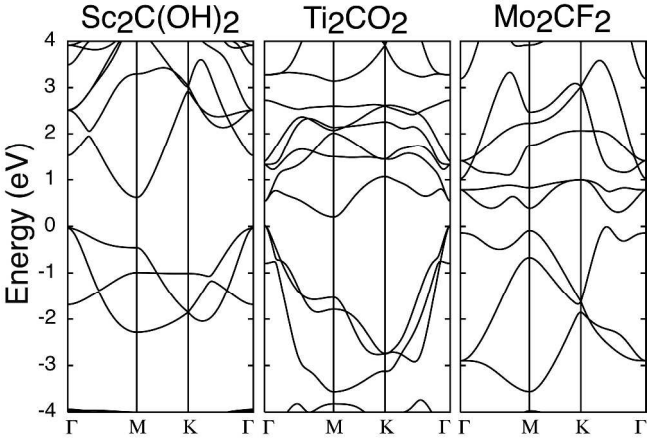

Though all semiconducting MXenes attain large Seebeck coefficients (>100 μV/K at 400 K), just some of them hold high electrical conductivities near the band edges. The reason for the

higher electrical conductivity of semiconducting Mo_2CF_2, $Mo_2C(OH)_2$, and Mo_2CCl_2 than other semiconducting MXenes, Sc_2CF_2, $Sc_2C(OH)_2$, Ti_2CO_2, Zr_2CO_2, and Hf_2CO_2, should be pursued in their different band structures. Since Ti, Zr, and Hf are in the same group of elements in the periodic table, Ti_2CO_2, Zr_2CO_2, and Hf_2CO_2 exhibit similar band structures.[24] Therefore, as typical band structures of semiconducting MXenes, only those of Ti_2CO_2, $Sc_2C(OH)_2$ and Mo_2CF_2 are shown in Fig. 5. Basically, the electrical conductivity is proportional to multiplication of the relaxation time, DOS and squared band velocities. Here, the relaxation time is set to be a constant for all MXenes. From Fig. 5, it is seen that top valence bands of Ti_2CO_2 might have larger band velocities than those of $Sc_2C(OH)_2$ and Mo_2CF_2, but its related DOS is broad, almost 20 times smaller than that of Mo_2CF_2 near the band edge at -0.05 eV. The higher electrical conductivity of Mo_2CF_2 than other semiconductors is attributed to its peculiar band structures. In this structure, the portions just below the valence band maximum (t_{2g}) are relatively flat (Γ to M points and K to Γ) and other portions are linearly dispersive (M to K). Hence, when the Fermi level locates near the valance band maximum of such band structure, relatively large Fermi surface is constructed, which holds a relatively large Fermi velocity. Consequently, Mo_2CF_2 obtain a higher electrical conductivity than Ti_2CO_2 and $Sc_2C(OH)_2$. Such a peculiar band shape is desirable for high performance thermoelectric devices, as it has already been pointed out for cobaltates (Na_xCoO_2)[43] referring as the "pudding mold" band type model[44,45] and for PbTe as the Kane-like band edges.[41] Based on above band models, a general rule for designing high efficient thermoelectric materials was proposed: a large Seebeck coefficient and a low resistivity consequently a large thermo factor is obtained in the materials with a band that is combined of relatively flat and relatively dispersive portions, when the chemical potential lies close to the band edges.[46-48]

Despite Cr is in the same group as Mo in the periodic table, most of functionalized Cr_2C systems are magnetic compounds.[24] Current version of BoltzTrap code is restricted to analyses the thermoelectric properties of nonmagnetic systems. Hence, we performed a set of thermoelectric calculations on *nonmagnetic* structures of monolayer and multilayer structures of functionalized Cr_2C with F, Cl, Br, OH, O, and S. It is observed that the band structure of a *nonmagnetic* functionalized Cr_2C system is similar to the functionalized Mo_2C system upon the same surface functionalization; multilayers Cr_2CF_2, Cr_2CCl_2, $Cr_2C(OH)_2$ are semiconductors with energy gaps of 0.22, 0.15 and 0.025 eV, respectively. They, thereby, obtain excellent thermo powers similar to the semiconducting Mo_2C systems. However, the Cr_2CBr_2, Cr_2CO_2, and Cr_2CS_2 with metallic properties obtain poor thermo powers. The results of the band structures and thermoelectric properties of nonmagnetic Cr_2C systems are included into the supplementary data.

Our theoretical predictions about the exceptional thermoelectric properties of Mo_2C-MXenes are consistent with other theoretical predictions and experimental results on other two-dimensional systems containing Mo. In this regard, 2D-MoS_2 has a high thermoelectric efficiency at room temperature relative to the other chalcogenides (WS_2 and WSe_2).[49] It has been demonstrated experimentally that MoS_2 deserves a remarkable performance in transistors due to its high electron mobility.[50-52] It was also reported that the electron mobility of 2D-MoO_3 exceeds that of MoS_2.[53]

Conclusions

Using the Boltzmann theory and first-principles electronic structure calculations, we have predicted the thermoelectric properties of more than 35 different functionalized MXene monolayers and their corresponding multilayers so as to identify the potential thermoelectrics in this newly discovered family of two-dimensional materials. In general, V-, Nb-, and Ta-based MXenes are good electrical conductors, but rather poor thermoelectrics. Ti-, Zr-, and Hf-based MXenes comprise average thermoelectrics. Mo- and semiconducting nonmagnetic Cr-based MXenes attain the best thermoelectric properties among all MXenes. In particular, Mo_2CF_2 is the most promising one. The remarkable thermoelectric properties of Mo_2CF_2 result from its semiconducting band gap and its peculiar band shape near the band edges. Moreover we have systematically studied how the electronic properties and the formation energies of the Mo_2C are affected by different F, Cl, Br, OH, O, and S functionalization.

Notes and references

[a] Computational Materials Science Unit, National Institute for Materials Science (NIMS), 1-1 Namiki, Tsukuba 305-0044, Ibaraki, Japan. E-mail: khazaei.mohammad@nims.go.jp.

[b] Computational Materials Science Unit, National Institute for Materials Science (NIMS), 1-2-1 Sengen, Tsukuba 305-0047, Ibaraki, Japan.

[c] International Center for Young Scientists (ICYS), National Institute for Materials Science (NIMS), 1-2-1 Sengen, Tsukuba 305-0047, Ibaraki, Japan.

[d] Materials Processing Unit, National Institute for Materials Science (NIMS), 1-2-1 Sengen, Tsukuba 305-0047, Ibaraki, Japan.

† Electronic Supplementary Information (ESI) available: [Crystal structures of the studied monolayers and multilayers, and their related electronic and thermolecetric properties]. See DOI: 10.1039/b000000x/

1 J. R. Sootsman, D. Y. Chung, M. G. Kanatzidis, *Angew. Chem. In. Ed.* 2009, **48**, 8616.
2 G. D. Mahan, *Solid State Phys.* 1998, **51**, 81.
3 F. J. DiSalvo, *Science* 1999, **285**, 703.
4 D. Parker, D. J. Singh, *J. Appl. Phys.* 2010, **108**, 083712.
5 Z. M. Sun, *Int. Mater. Rev.* 2011, **56**, 143.
6 M. W. Barsoum, *Prog. Solid State Chem.* 2000, **28**, 201.
7 M. W. Barsoum, H. -I. Yoo, I. K. Polushina, V. Yu. Rud', T. El-Raghy, *Phys. Rev. B* 2000, **62**, 10194.
8 H. -I. Yoo, H. W. Barsoum, T. El-Raghy, *Science* 2000, **407**, 581.
9 L. Chaput, G. Hug, P. Pécheur, H. Scherrer, *Phys. Rev. B* 2007, **75**, 035107.
10 L. Chaput, G. Hug, P. Pécheur, & H. Scherrer, *Phys. Rev. B* 2005, **71**, 121104.
11 M. Naguib, M. Kurtoglu, V. Presser, J. Lu, J. Niu, M. Heon, L. Hultman, Y. Gogotsi, M. W. Barsoum, *Adv. Mater.* 2011, **23**, 4248.
12 M. Naguib, O. Mashtalir, J. Carle, V. Presser, J. Lu, L. Hultman, Y. Gogotsi, M. W. Barsoum, *ACS Nano* 2012, **6**, 1322.
13 M. Naguib, J. Halim, J. Lu, K. M. Cook, L. Hultman, Y. Gogotsi, M. W. Barsoum, *J. Am. Chem. Soc.* 2013, **135**, 15966.
14 M. R. Lukatskaya, O. Mashtalir, C. E. Ren, Y. Dall'Agnese, P. Rozier, P. L. Taberna, M. Naguib, P. Simon, M. W. Barsoum, Y. Gogotsi, *Science* 2013, **341**, 1502.
15 O. Mashtalir, M. Naguib, V. N. Mochalin, Y. D. Agnese, M. Heon, M. W. Barsoum, Y. Gogotsi, *Nature Commun.* 2013, **4**, 1716.
16 F. Chang, C. Li, J. Yang, H. Tang, M. Xue, *Mater. Lett.* 2013, **109**, 295.
17 X. Zhang, J. Xu, H. Wang, J. Zhang, H. Yan, B. Pan, J. Zhou, Y. Xie, *Angew. Chem Int. Ed.* 2013, **52**, 4361.
18 N. Enyashin, A. L. Ivanovskii, *Comput. Theor. Chem.* 2012, **989**, 27.

19 I. R. Shein, A. L. Ivanovskii, *Comput. Mater. Sci.* 2012, **65**, 104.
20 M. Kurtoglu, M. Naguib, Y. Gogotsi, M. W. Barsoum, *MRS Commun.* 2012, **2**, 133.
21 A. N. Enyashin, A. L. Ivanovskii, *J. Phys. Chem. C* 2013, **117**, 13637.
22 Q. Tang, Z. Zhou, P. Shen, *J. Am. Chem. Soc.* 2012, **134**, 16909.
23 Y. Xie, P. R. C. Kent, *Phys. Rev. B* 2013, **87**, 235441.
24 M. Khazaei, M. Arai, T. Sasaki, C. –Y. Chung, N. S. Venkataramanan, M. Estili, Y. Sakka, Y. Kawazoe, *Adv. Funct. Mater.* 2013, **23**, 2185.
25 L. Gan, D. Huang, U. Schwingenschlögl, *J. Mater. Chem. A* 2013, **1**, 13672.
26 G. S. Nolas, J. Sharp, H. J. Goldsmid, *Thermoelectrics: basic principles and new materials developments*, Springer, Berlin, Germany 2001.
27 J. P. Perdew, K. Burke, M. Ernzerhof, *Phys. Rev. Lett.* 1996, **77**, 3865.
28 G. Kresse, J. Furthmu□ller, *Comput. Mater. Sci.* 1996, **6**, 15.
29 M. Methfessel, A. T. Paxton, *Phys. Rev. B* 1989, **40**, 3616.
30 H. J. Monkhorst, J. D. Pack, *Phys. Rev. B* 1976, **13**, 5188.
31 G. K. H. Madsen, D. J. Singh, *Comput. Phys. Commun.* 2006, **175**, 67.
32 G. K. H. Madsen, *J. Am. Chem. Soc.* 2006, **128**, 12140.
33 J. Yang, H. Li, T. Wu, W. Zhang, L. Chen, J. Yang, *Adv. Funct. Mater.* 2008, **18**, 2880.
34 M. Khazaei, M. Arai, T. Sasaki, M. Estili, Y. Sakka, *Sci. Tech. Adv. Mater.* 2014, in press.
35 L. F. Mattheis, *Phys. Rev. B* 1973, **8**, 3719.
36 L. D. Hicks, M. S. Dresselhaus, *Phys. Rev. B* 1993, **47**, 12727.
37 M. Zebarjadi, K. Esfarjani, M. S. Dresselhaus, Z. F. Ren, G. Chen, *Energy Environ. Sci.* 2012, **5**, 5147.
38 M. Zebarjadi, K. Esfarjani, Z. Bian, A. Shakouri, *Nano Lett.* 2011, **11**, 2225.
39 L. Hao, T. K. Lee, *Phys. Rev. B* 2010, **81**, 165445.
40 M. Onoue, F. Ishii, T. Oguchi, *J. Phys. Soc. Jpn. 2008,* **77**, 054706.
41 D. J. Singh, *Phys. Rev. B* 2010, **81**, 195217.
42 L. Zhang, D. J. Singh, *Phys. Rev. B* 2009, **80**, 075117.
43 D. J. Singh, D. Kasinathan, *J. Electron. Mater.* 2007, **36**, 736.
44 K. Kuroki, R. Arita, *J. Phys. Soc. Jpn.* 2007, **76**, 083707.
45 P. Wissgott, A. Toschi, G. Sangiovanni, K. Held, *Phys. Rev. B* 2011, **84**, 085129.
46 A. F. May, D. J. Singh, G. J. Snyder, *Phys. Rev. B* 2009, **79**, 153101.
47 D. J. Singh, I. I. Mazin, *Phys. Rev. B* 1997, **56**, 1650.
48 D. J. Singh, *Phys. Rev. B* 2010, **81**, 195217.
49 W. Huang, H. Da, G. Liang, *J. Appl. Phys.* 2013, **113**, 104304.
50 M. Chhowalla, H. S. Shin, G. Eda, L. –J. Li, K. P. Loh, H. Zhang, *Nat. Chem.* 2013, **5**, 263.
51 B. Radisavljevic, A. Radenovic, J. Brivio, V. Giacometti, A. Kis, *Nat. Nanotech.* 2011, **6**, 147.
52 B. Radisavljevic, A. Kis, *Nat. Mater.* 2013, **12**, 815.
53 S. Balendhran, J. Deng, J. Z. Ou, S. Walia, J. Scott, J. Tang, K. L. Wang, M. R. Field, S. Russo, S. Zhuiykov, M. S. Strano, N. Medhekar, S. Sriram, M. Bhaskaran, K. Kalantar-zadeh, *Adv. Mater.* 2013, **25**, 109.

